Singlet and Triplet Valence Excited States of Pyrimidine

Gad Fischer,[†] Zheng-Li Cai,[‡] Jeffrey R. Reimers,*[,‡] and Paul Wormell[§]

Department of Chemistry, The Faculties, Australian National University, Canberra 0200, Australia, School of Chemistry, The University of Sydney, NSW 2006, Australia, and Centre for Biostructural and Biomolecular Research, University of Western Sydney, NSW 1797, Australia

Received: September 25, 2002; In Final Form: January 29, 2003

The absorption spectrum of pyrimidine vapor at 75 °C in the region of the first singlet−triplet transition, encompassing hot bands of the first singlet−singlet transition, has been obtained and analyzed with the aid of extensive ab initio (EOM-CCSD, CASPT2, and CIS) and density functional (B3LYP and TD-B3LYP) vibrational analyses. The hot bands in these spectra give information about low-frequency vibrations, several of which are vibronically active but are not particularly effective at inducing intensity. Spectra obtained at 18 °C are also reported for up to 1100 cm^{-1} above the singlet−singlet origin. Several singlet−singlet hot bands have been reassigned, giving excited-state vibrational frequencies for some modes. The calculations provide not only quantitative verification of perceived vibronic coupling and other features of the experimental assignments but also detailed maps of the complex lowest singlet and triplet manifolds. This includes vertical and adiabatic excitation energies, relaxation energies, excess spin densities, and normal-mode vibrational displacement and Duschinsky rotation analyses for up to eight singlet and eight triplet excited states as well as estimates for the structure and energy of some important interconnecting transition states and conical intersections. As a result, revised assignments for the majority of the triplet states are suggested. In addition, the pseudoparity selection rule, which forms the primary model for the (π^*, π) spectroscopy of alternate conjugated hydrocarbons, is found not to apply to the $^3A_1$ manifold. The possibility of symmetry breaking in the (π^*, n) states caused by vibronic coupling to a_2 vibrations is considered in detail, as is the possibility of the excited states taking the nonplanar "boat" configuration because of vibronic coupling in b_1 modes. Excited-state chemical properties such as reaction rates and hydrogen bonding are very sensitive to these effects.

1. Introduction

Interest in the electronic spectroscopy of the azabenzenes[1] is undergoing a renaissance due to their rich excited-state dynamical and photochemical properties[2,3] and their importance as models for biologically relevant spectroscopic processes[4,5] and because they serve as admirable model systems for new ab initio and density functional calculations of excited electronic states. (See, for example, refs 6−12.) These reasonably small, symmetric, and well-studied heterocycles have a range of distinctive and experimentally accessible excited electronic states, many of which have been detected and, in some cases, studied in detail. Their vibrational spectra are also fairly well characterized. They continue to give new insights into the vibronic interactions, radiationless processes, and solvation properties of heterocyclic molecules.

Pyridine, the diazines, the triazines, and *s*-tetrazine have a variety of singlet and triplet states, both (π^*, π) and (π^*, n), that are experimentally accessible.[1,2,13,14] In many cases, the states are well separated and readily characterized, but there are some instructive exceptions, notably pyridine[2,3] and pyridazine.[13] The excited singlet states are, in most cases, fairly well characterized, but the triplet states are less so. A variety of ab initio calculations have been carried out on triplet states,[3,11,13,15−17] but for pyrimidine, very little is known and improved computational and experimental data are required. Secure assignments of excited electronic states, together with the knowledge of their potential surfaces, are also relevant to studies of radiationless transitions within these molecules. (See pyridine, for example.)

This paper presents new experimental data for the lowest excited singlet and triplet states of pyrimidine; new high-level calculations are presented for the first eight singlet and triplet valence excited states. In its ground state, pyrimidine belongs to the C_{2v} point group, so its (π^*, π) states have A_1 or B_2 symmetry whereas its (π^*, n) states are A_2 or B_1. The first singlet−singlet absorption, $S_1 \leftarrow S_0$, is an allowed $^1B_1 \leftarrow {}^1A_1$ (π^*, n) transition, with vibronic development predominantly in totally symmetric (a_1) modes; it also has a prominent Fermi resonance between one quantum of the 6a (a_1) mode and two quanta of the 6b (b_2) mode.[1,18] The numbering convention that we use for the normal vibrational modes of pyrimidine follows Lord's scheme.[19] In the term $6a_0^1$, the superscript 1 is the number of quanta of mode 6a that are excited in the upper electronic state, and the subscript 0 is the number excited in the lower state. Thus, $6a_0^1$, $6a_1^0$, and $6a_1^1$ are a cold band, a hot band, and a sequence band, respectively.

Previously, the singlet−triplet absorption spectrum of pyrimidine has been recorded in the pure crystal at 4.2 K by Hochstrasser and Marzzacco[20] and at 1.2 K by Nonhof and van der Waals,[21] through gas-phase phosphorescence by Takemura et al.,[22] and by phosphorescence excitation in the gas phase by Fujita et al.[23] as well as in a molecular beam by Ottinger, Vilesov, and Winkler.[24] The rotational contours of the molec-

* To whom all correspondence should be addressed. E-mail: reimers@chem.usyd.edu.au. Tel: +61 2 9351 4417. Fax: +61 2 9351 3329.
[†] Australian National University.
[‡] The University of Sydney.
[§] University of Western Sydney.

10.1021/jp0221385 CCC: $25.00
Published on Web 04/05/2003

ular-beam spectrum indicate that the lowest-energy triplet band system, $T_1 \leftarrow S_0$, is due to a $^3B_1 \leftarrow {}^1A_1$ (π^*, n) transition and suggest that the S_1 and T_1 states have similar geometries. Similar conclusions were reached by Hochstrasser and Marzzacco[20] from the pure-crystal spectra. As for the singlet−singlet system, the distinctive vibronic development involves only a_1 modes. These results imply that S_1 and T_1 both have full C_{2v} symmetry but are insufficient to guarantee that the potential energy surfaces do not have double-well structures whose asymmetric minima are too shallow to support zero-point vibration. In fact, it is conceivable that such double-well potentials could occur in *any* of the a_2, b_1, or b_2 symmetries, and secure vibrational analysis provides the best means of resolving these questions. Because chemical properties of the excited states such as reaction rates and hydrogen bonding strengths are altered dramatically if the potential surface has a double minimum, the resolution of this issue is quite important.

Several higher-energy singlet states have been located for pyrimidine. Some earlier assignments have been reviewed,[1] and others have been proposed by Palmer and co-workers.[17] Less is known about the higher triplet states since they are obscured by strong singlet−singlet absorption in the normal absorption spectrum. A few triplet−triplet absorption bands have been reported in water solution,[25] but the ordering and energies of the excited states are likely to be substantially different from those in the vapor phase. Walker, Palmer, and co-workers[17,26−29] have carried out a comprehensive and detailed survey of vacuum UV and UV−visible absorption and photoelectron and near-threshold electron energy-loss (EEL) spectra of the azines, including pyrimidine, and have analyzed their results using ab initio MRDCI and CASSCF calculations. An advantage of the EEL spectra is that they locate triplet as well as singlet states. However, the spectra are complex, and some important states—notably the well-known $^1B_1(\pi^*, n)$ S_1 state of pyrimidine and the lowest $^3A_1(\pi^*, \pi)$ state—are not apparent. On the basis of more modern calculations, we provide an extensive reassignment of the bands observed in the EEL spectra.

Further experimental studies of the excited states are required to confirm some of the higher-energy triplet assignments, particularly in regions where the density of electronic states is high. An alternative way of obtaining information about the ordering and relative energies of excited states is to study the extent of vibronic coupling within the singlet and triplet manifolds. For example, the low-energy $^3B_1$ (π^*, n) state of pyrimidine can couple with nearby $^3A_1$ (π^*, π), $^3A_2$ (π^*, n), $^3B_1$ (π^*, n), and $^3B_2$ (π^*, π) states through vibrational modes with b_1, b_2, a_1, and a_2 symmetries, respectively. In-plane modes have a_1 or b_2 symmetry; out-of-plane modes are a_2 or b_1. Several low-frequency vibrations are vibronically active in both the singlet and triplet manifolds, but they are not effective at inducing intensity in the normal absorption spectrum. However, their excited-state frequencies show substantial perturbations, which reflect the size of the vibronic-coupling matrix elements and the energy gaps between the coupled electronic states. Thus, the way in which vibrational frequencies differ among the ground and excited states can give useful information about the energy gaps between the coupled states. For a compound such as pyrimidine, in which nontotally symmetric vibrations contribute little to the absorption spectrum, information about their energies in the excited state can be obtained from the sequence structure on the origin and other strong bands as well as the Fermi resonances that occur. It is also possible that nontotally symmetric modes may be vibronically active to the extent that the excited-state potential energy surfaces have shallow double-minimum structures, giving rise to symmetry-breaking effects. Such molecular deformations would be evidenced by the anharmonicity of the vibrational modes concerned. Similar studies of the sequence bands in the $T_1 \leftarrow S_0$ spectra of pyrazine[14] and pyridazine[13] have been instructive, providing additional experimental evidence to correlate with computational studies. Earlier studies of pyrimidine paid relatively little attention to sequence and other hot bands, although some assignments were proposed, but recent developments in theory now make it possible to calculate excited-state vibrational frequencies, which in turn makes a thorough analysis of these bands both feasible and instructive.

There have been several studies of the absorption and fluorescence spectra of pyrimidine and its perdeuterated analogue, pyrimidine-d_4. Innes et al.[30] reported and analyzed the high-resolution $S_1 \leftarrow S_0$ spectra of the -d_0 and -d_4 compounds; their study encompassed rotational contours, Fermi resonances, and the Franck−Condon behavior of the spectrum. Single vibronic-level fluorescence (SVLF) spectra were reported by Knight et al.[18] and O'Brien et al.[31] for pyrimidine-d_0 and pyrimidine-d_4, respectively, with the most recent assignments due to Pongor et al.[32] being based on a combination of this body of work and an a-priori force-field analysis. We have reanalyzed the spectra of the deuterated molecule in light of the new assignments for pyrimidine-h_4 and have made some new assignments. (See section 5C.)

Similarities between the $^1B_1$ (π^*, n) S_1 and $^3B_1$ (π^*, n) T_1 states of pyrimidine, referred to above, make it worthwhile to compare the hot-band regions of the singlet−singlet and singlet−triplet absorption spectra. For this molecule, vibronic coupling strengths (in nontotally symmetric modes) are naively expected to be similar for the singlet and triplet manifolds, moderated only by differing energy gaps between the interacting states, where significant energy-gap changes are expected only for the interaction with the A_1 states via b_1 modes. Since the excited singlet states are fairly well characterized, a comparison of excited-state vibrational frequencies should give useful information about the relative energies of the higher-energy triplet states, some of which have not been detected spectroscopically. This additional experimental information we use to confirm the features of our computationally based assignments for the higher triplet states; however, lines observed in the spectra for which the interpretation is not clear are assigned on the basis of computed values.

Experimentally, the singlet−singlet hot bands of pyrimidine have been incompletely reported and analyzed,[30] and in the phosphorescence-excitation study,[24] the molecular beam was too cold for singlet−triplet hot bands to be seen. As may be seen below, the analysis of the singlet−singlet hot bands is by no means straightforward, owing to vibronic interactions associated with closely spaced singlet excited states and also anharmonic coupling (Fermi resonance) between some vibronic levels. A further interesting comparison may be made with pyridazine, in which the vibronic development of the $T_1 \leftarrow S_0$ spectrum is simple but the corresponding $S_1 \leftarrow S_0$ absorption is heavily perturbed.[13] In contrast, both corresponding spectra for pyrimidine appear to be uncomplicated.

Traditionally,[6−12] computational studies of azines have focused mainly on the evaluation of vertical excitation energies, with the aims of both spectral assignment and verification of the quality of the computational model. Such studies include semiempirical CNDO,[33] configuration interaction with single excitations (CIS),[8] complete active-space self-consistent field[34] (CASSCF) with second-order Møller−Plesset correction

TABLE 1: Calculated and Observed Bond Lengths and Bond Angles for Selected States of Pyrimidine[a]

state	method	symmetry	N−C$_1$	N−C$_3$	C$_3$−C$_4$	N−C$_1$−N	C$_1$−N−C$_3$	N−C$_3$−C$_4$	C$_3$−C$_4$−C$_3$	θ	ϕ
$^1A_1$	CCSD	C_{2v}	1.345	1.345	1.401	128	115	123	116	0	0
$^1A_1$	obsd[b]	C_{2v}	1.328	1.350	1.393	128	116	122	117	0	0
$^1B_1$	EOM-CCSD	C_{2v}	1.326	1.395	1.402	118	123	119	118	0	0
$^1A_2$	EOM-CCSD	C_{2v}	1.382	1.304	1.436	112	126	123	111	0	0
$^1A_2$	EOM-CCSD	C_s	1.389	1.305	1.432	111	126	123	111	9	2
$^3B_1$	EOM-CCSD	C_{2v}	1.328	1.394	1.401	119	123	118	118	0	0
$^3B_1$	EOM-CCSD	C_s	1.334	1.404	1.401	120	121	119	118	15	4
$(\alpha)^3A_1$	EOM-CCSD	C_{2v}	1.421	1.301	1.484	127	116	122	116	0	0
$(\alpha)^3A_1$	EOM-CCSD	C_s	1.420	1.299	1.485	124	114	121	114	28	21
$(\beta)^3A_1$	EOM-CCSD	C_{2v}	1.352	1.452	1.406	129	115	121	119	0	0
$^3A_2$	EOM-CCSD	C_{2v}	1.388	1.306	1.429	112	125	123	112	0	0
$^3A_2$	EOM-CCSD	C_s	1.399	1.308	1.424	110	126	123	112	11	1

[a] All calculations are performed using the cc-pVDZ basis set. The bond lengths are in angstroms, and angles are in degrees; full coordinates and geometrical properties for all states are given in Supporting Information. [b] From refs 1 and 55.

(CASPT2),[8] equation-of-motion coupled cluster with single and double excitations (EOM-CCSD)[10] with the inclusion of triple excitations (EOM-CCSD(T)),[10] similarity-transformed EOM-CCSD (STEOM-CCSD),[11] and density functional[9] studies. Our studies of the singlet states of pyridazine,[13] pyrazine,[16] and pyridine[3] show that calculations of vertical excitation energies alone are not sufficient when analyzing the spectra of molecules of this complexity; indeed, they may potentially be misleading. This is particularly pertinent, for example, when considering the origin bands for transitions in which the electronic transition causes a significant change in molecular geometry. However, adiabatic calculations, in which energies are calculated for the optimized excited-state geometry, have given very satisfactory results. Furthermore, the difference between the vertical and adiabatic energies, known as the *reorganization* energy λ_E, is an important, readily accessible characteristic of an absorption band and should be considered when making band assignments.

In assigning the observed spectra, we consider calculated vertical excitation energies and adiabatic energies as well as calculated vibrational frequencies and Duschinsky matrices. Extensive qualitative agreement is found, and many assignments are made. In addition, we calculate properties for the lowest eight singlet and eight triplet states of pyrimidine, mapping out key sections of the lowest singlet and triplet manifolds, elucidating the chemistry of the excited states of pyrimidine.

2. Methods

2A. Experimental. Pyrimidine (Aldrich and Fluka purum grade) was used without further purification. The vapor absorption spectra were obtained in a 6-m multiple-reflection cell, with path lengths up to about 300 m, using a 450-W high-pressure xenon arc lamp as the light source. For the singlet−triplet spectra, the cell was held at temperatures up to 75 °C, with the end plates a few degrees hotter. Singlet−singlet spectra were measured at 18 °C. The spectra were recorded photographically in the first order of a 590 grooves/mm grating blazed at 400 nm using a Jarrell-Ash 3.4-m grating spectrograph. Calibration was by the iron lines of an iron hollow-cathode lamp. Plates were traced using a Joyce-Loebl Mark IIIC scanning microdensitometer. Higher-resolution spectra were recorded using the seventh order of a 600 grooves/mm grating blazed at 2500 nm.

In addition to the spectra shown in the Results section, a multitude of additional spectra were recorded over a wide temperature range using samples exposed to radiation for 30 s to 3 h both with and without the use of filters to remove unwanted incident light. These spectra provide unambiguous assignments of observed peaks to either cold bands or hot bands and indicate that no reported bands arise from photochemical decomposition products.

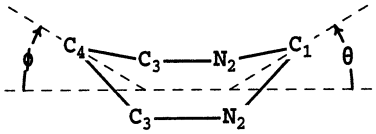

Figure 1. Boat distortion predicted for many of the excited states of pyrimidine.

2B. Computational. Calculations were performed with the cc-pVDZ basis set[35] by the following methods: coupled-cluster singles and doubles[36] (CCSD) using ACES-II,[37] equations of motion CCSD[38] (EOM-CCSD) using ACES-II,[37] complete-active-space self-consistent field[34] (CASSCF) using DALTON,[39] CASSCF with second-order perturbation theory corrections[40] (CASPT2) using MOLCAS,[41] density functional theory (DFT) with the B3LYP functional[42] using Gaussian 98,[43] and time-dependent DFT (TD-DFT)[9] with the B3LYP functional[42] (TD-B3LYP) using TURBOMOLE.[44] In addition, configuration-interaction singles[45] (CIS) calculations were performed with the 6-31G* basis set using Gaussian 98.[43] For the TD-DFT and CASPT2 methods, numerical second derivatives were evaluated using our own program; this program was also used to correct for errors produced by ACES-II in the b_2 vibrational frequencies found for approximately half of the states studied. Details of the active spaces used in the CASSCF and CASPT2 calculations are given in Supporting Information.

3. Overview of Computational Results for the Singlet and Triplet Manifolds

3A. General Features. Details of the EOM-CCSD, CCSD, TD-B3LYP, B3LYP, CASSCF, CASPT2, and CIS calculated properties of the ground state and the lowest eight excited singlet and eight triplet states of pyrimidine are provided in full in Supporting Information. These include electronic-state, transition-state, and conical-intersection geometries and energies, rotational constants, and excess spin densities, and, for most electronic states, normal modes, normal-mode displacements, and Duschinsky matrices. The Duschinsky matrices are obtained using normal coordinates; for large-amplitude torsional modes, the use of curvilinear coordinates is more appropriate,[46] and the material provided is in a format that may readily be reprocessed if required. A summary of key geometric information is given in Table 1, including the out-of-plane torsional angles θ and ϕ defined in Figure 1 that specify values for possible out-of-plane "boat" deformations of pyrimidine.

Calculated vertical excitation energies are shown in Table 2, where they are compared with experiment and the results of previous calculations. Calculated 0−0 transition energies are given in Table 3, with the associated excited-state reorganization energies λ_E provided in Table 4 and the zero-point energy (ZPE)

TABLE 2: Calculated and Observed Vertical Excitation Energies (eV) for Pyrimidine

method	basis	$^1B_1$	$^1A_2$	$^1B_2$	$(2)^1A_2$	$(2)^1B_1$	$(2)^1A_1$	$(3)^1A_1$	$(2)^1B_2$	$^3B_1$	$^3A_1$	$^3A_2$	$^3B_2$	$(2)^3A_1$	$(2)^3A_2$	$(2)^3B_1$	$(2)^3B_2$	error[d]
CCSD	cc-pVDZ									4.36	4.59	4.98	5.15	4.90	5.91	6.48	6.37	0.51
EOM-CCSD	cc-pVDZ	4.74	5.10	5.52	6.31	6.60	7.20	8.10	8.33	4.28	4.29	4.83	5.08	5.45	5.81	6.38	6.68	0.45
CASPT2	cc-pVDZ	4.26	4.49	5.17		6.03	7.10			3.81	4.35	4.24	4.83	5.13	5.39	5.93	6.51	0.16
B3LYP	cc-pVDZ									3.92	4.70	4.40	4.87	5.00	5.32	5.70	6.00	0.06
TD-B3LYP	cc-pVDZ	4.31	4.55	5.87	5.75	5.94	6.69	7.73	7.75	3.73	4.11	4.19	4.76	5.25	5.13	5.60	5.98	0.22
CIS	6-31G*	6.02	6.69	6.81	7.71	8.94	7.24	9.12	9.35	5.15	3.98	5.84	5.10	5.79	7.17	7.98	6.89	1.71
CASSCF[a]	ANO[b]	5.22	5.83	5.21	6.92	7.41	7.30	8.15	8.55									0.88
CASSCF[ck]	ANO[b]	5.61	6.22	5.25			7.68	9.26	9.26									1.29
CASPT2[c]	ANO[b]	3.81	4.12	4.93			6.72	7.57	7.57									0.38
MRCI[a]	ANO[b]	3.82	4.22	5.53	5.70	6.12	6.96	7.67	8.21									0.36
MRDCI[i]	DZ+Ryd[i]	3.74	4.19	4.71			8.07			3.68	3.90	3.90	4.75					0.65
EOM-CCSD[d]	sadlej[e]	4.62	5.03	5.44	6.17	6.50	6.95	7.73	8.10									0.30
EOM-CCSD(T)[d]	sadlej[e]	4.24	4.74	5.01	5.84	6.11	6.57	7.35	7.82									0.18
STEOM-CCSD[f]	sadlej[e]	4.40	4.72	5.04	5.94	6.18	6.87	7.44	7.77									0.14
CCSDresp.[j]	sadlej[e]	4.59	5.16			6.51	7.01	7.73										0.30
obsd (old assignments)		4.2[g]	4.6[g]	5.2[i]	5.7[i]	6.0[i]	6.7[gi]	7.57[i]	7.57[i]	3.6[i]		~4.5[i]	5.05[i]					
obsd (new assignments)										>3.6		4.2	4.7	5.0	5.3	~5.6		
obsd (ZPE-corrected[h])		4.3	4.8	5.3	5.9	6.1	6.8	7.6	7.6	>3.8[m]		4.4	4.8	5.1	5.4	5.7		

[a] From ref 7. [b] Large atomic natural orbital; see ref 8. [c] From ref 8. [d] From ref 10. [e] Basis functions (180) from ref 56. [f] From ref 11. [g] From ref 48. [h] Corrected for zero-point energy (ZPE). [i] From ref 17. [j] Coupled cluster response theory.[57] [k] See also ref 6. [l] Root-mean-square (RMS) error between calculated and ZPE corrected observed values. [m] 4.0 used in RMS analysis.

TABLE 3: Calculated and Observed 0−0 Energy Differences E_{00} (eV) to the Ground State of Pyrimidine

method	$^1B_1$	$^1A_2$	$^1B_2$	$(2)^1A_2$	$(2)^1B_1$	$(2)^1A_1$	$(3)^1A_1$	$(2)^1B_2$	$^3B_1$	$(\alpha)^3A_1$	$(\beta)^3A_1$	$^3A_2$	$^3B_2$	$(2)^3A_1$	$(2)^3A_2$	$(2)^3B_1$	$(2)^3B_2$
CCSD									3.69[a]	3.63[a]	3.91[a]	4.03[a]	4.80[a]		5.21[a]	6.12[a]	6.09[a]
EOM-CCSD	4.17[l]	4.19[f]	5.29[f]	5.56[f]	6.21[l]	6.69	7.80[a]	8.10	3.61[fm]	3.64[f]	3.90[hl]	3.91[f]	4.71	5.27[a]	5.36[a]	6.05[a]	6.46[a]
CASPT2	3.56[ab]								3.10[ab]								
B3LYP	3.74[ail]								3.30	3.64[f]	4.01[jl]	3.47[f]	4.56[k]		4.63[k]	5.37[kl]	5.72[k]
CIS	5.32	5.61[f]	6.48	7.28	8.14	6.73	8.83	8.98	4.53	3.31	x[g]	4.96[fmn]	4.79[jk]	5.50[jl]	6.75[kl]	7.70[k]	6.53[k]
obsd−old assn.	3.85[c]	4.07[c]	5.00[c]		~5.7[d]	6.49[e]	7.25[c]	7.25[c]	3.54[c]								
obsd−new assn.						6.26											

[a] Obtained using best-estimate zero-point energy corrections; see Supporting Information. [b] b_1 displacements not considered. [c] From ref 1. [d] Estimated from the spectra of ref 17. [e] From ref 48. [f] Evaluated at optimized "boat" structure with C_s symmetry. [g] Not a local minimum; collapses to $(\alpha)^3A_1$. [h] Neglecting the mode of the imaginary frequency, which leads to $(\alpha)^3A_1$ without a barrier. [i] TD-B3LYP. [j] Anharmonic analysis for the a_2 double well. [k] Anharmonic analysis for the b_1 double well. [l] Anharmonic analysis for the b_2 double well. [m] Anharmonic analysis for the a″ double well. [n] No a_2 or b_2 double well at the C_{2v} structure.

TABLE 4: Calculated and Observed Excited-State Reorganization Energies, λ_E (eV), after Vertical Excitation from the Ground State of Pyrimidine

method	sym.[b]	$^1B_1$	$^1A_2$	$^1B_2$	$(2)^1A_2$	$(2)^1B_1$	$(2)^1A_1$	$(3)^1A_1$	$(2)^1B_2$	$^3B_1$	$(\alpha)^3A_1$	$(\beta)^3A_1$	$^3A_2$	$^3B_2$	$(2)^3A_1$	$(2)^3A_2$	$(2)^3B_1$	$(2)^3B_2$
CCSD	C_{2v}									0.49	0.77	0.44	0.77	0.22		0.57	0.30	0.25
EOM-CCSD	C_{2v}	0.46	0.74	0.19	0.57	0.29	0.42	0.28	0.21	0.45	0.46	0.15	0.69	0.20	0.18	0.32	0.27	0.19
EOM-CCSD	C_s	0	0.045	0	[0.024][a]	0.50	0		[0.138][a]	0.019	0.038	0.51[e]	0.045	0			[0.005][a]	
CASPT2	C_{2v}	0.5								0.42								
B3LYP	C_{2v}									0.44	0.76	0.45	0.72	0.23		0.56	0.27	0.25
B3LYP	C_s									0	0.105	0	0.033					
CIS	C_{2v}	0.53	0.85	0.17	0.38	0.77	0.34	0.25	0.24	0.47	0.45	[k]	0.61	0.22	0.18	0.18	0.22	0.27
CIS	C_s		0.04										0.09					
CASSCF[bc]	C_{2v}									0.41	0.39		0.53					
CASSCF[bc]	C_s									0.01	0		0					
obsd[d]		0.35[ghi]	~0.6[fgj]	0.20[ghj]	>0.4[fi]	~0.3[j]	0.44[fh]	0.32[gj]	0.32[gj]	>0.1			0.5[j]					

[a] Estimated by displacement in the mode of imaginary frequency. [b] Either for relaxation within the C_{2v} point group or the *additional* relaxation following distortion to the "boat" structure; possible minor relaxations in other modes (see Supporting Information, Table 10) are not included. [c] From ref 6. [d] Our estimates. [e] Leads directly to $^3B_1$; see Figure 2. [f] Our interpretation of experimental spectra. [g] From ref 1. [h] From ref 48. [i] From ref 58. [j] From ref 17. [k] Leads to $(\alpha)^3A_1$ without barrier.

corrections provided in Supporting Information. In most cases, relaxation within the C_{2v} point group accounts for almost all of the reorganization energy. However, normal-mode analysis at the resultant geometries sometimes produces imaginary eigenvalues, indicating the presence of a double-well potential in one or more asymmetric modes. Large relaxations were found for b_1 modes only, often leading to boatlike structures as depicted in Figure 1. For these, explicit geometry optimizations in the lower (C_s) point group were performed, and the normal-mode analysis was repeated. In other cases, the double-well potentials were evaluated explicitly as a function of the appropriate normal-mode displacements, leading to the evaluation of revised harmonic and (diagonal) anharmonically corrected vibrational frequencies, zero-point energies, and estimated asymmetric contributions to the reorganization energy. These values are shown in Tables 2−4 and the Supporting Information, and the prediction of double wells is flagged in Table 3.

For $^3A_1$, the calculated potential energy surfaces have a double-well structure as a function of the totally symmetric normal coordinate Q_{8a}. The chemical significance of this is discussed in detail in section 3C. CCSD, EOM-CCSD, CASSCF, and B3LYP calculations all predict two separate minima for this state, and these are named $(\alpha)^3A_1$ and $(\beta)^3A_1$ in Tables 3 and 4 and so forth. From CIS calculations, the appearance of the higher-energy $(\beta)^3A_1$ minimum was apparent, but no local minimum was found.

3B. Comparing Observed and Calculated Vertical Excitation Energies. Observed 0−0 transition energies are also shown in Table 3 on the basis of existing assignments and our revised assignments (see below) of the observed spectra of pyrimidine. Related vertical excitation energies and reorganization energies are shown in Tables 2 and 4, though the most appropriate experimental values for these quantities are often not clear. Computed vertical transition energies correspond to the *average* band absorption energies[3] but are typically approximated simply by the observed band maxima. Correction of the calculated values for zero-point motion is also required, but because zero-point energy corrections are available only for a small subset of the computational methods used, we facilitate an improved comparison of observed and calculated data by determining a "best estimate" computed zero-point energy change for a particular state and adjusting the observed band maximum accordingly. We obtain these estimates as either the average of the available calculated B3LYP and EOM-CCSD values or calculated CIS values otherwise, as described in Supporting Information. The corrected experimental vertical excitation energies are shown Table 2, as are the root-mean-square (RMS) deviations between them and the calculated values.

In comparing the calculated and experimental vertical excitation energies, it is clear that the EOM-CCSD(T), STEOM-CCSD, CASPT2, B3LYP, and TD-B3LYP results are in excellent agreement with experiment, with RMS deviations of less than 0.25 eV. Because ZPE corrections are typically on the order of 0.1 to 0.2 eV and because average band energies can differ from band maxima by 0.1−0.2 eV, it is clearly important that these issues be addressed when comparing observed and calculated data. The CCSD and EOM-CCSD results differ from the adjusted experimental data by up to 0.5 eV; however, the difference is composed largely of a consistent overestimation of the excited-state energies, indicating that these methods remain appropriate for the calculation of the relative energy differences and hence the shapes of the potential energy surfaces, including the properties of transition states and conical intersections. Most important, all of these methods produce the same state ordering, with the exception of the incorrect ordering of $^1B_2/(2)^1A_2$ produced by TD-B3LYP and the ordering of the apparently nearly degenerate states $^3A_1$ and $^3A_2$.

The calculated reorganization energies are in realistic agreement with the experimental values for all states except $(2)^1B_1$. For this state, the observed band appears to be narrow, and a value of ca. 0.3 eV appears to be in order. The CIS calculations produce a large reorganization energy of 0.77 eV within the C_{2v} symmetry whereas the EOM-CCSD calculations predict 0.29 eV within C_{2v} with an additional 0.50 eV attributed to symmetry reduction to C_s symmetry. Although this could indicate that the experimental assignment is incorrect, it is more likely that this discrepancy arises from incorrect perceptions of the vibronic coupling involving $(2)^1B_1$ within the calculations.

3C. Breakdown of the Alternate-Polyene Model for $^3A_1$, the Lowest-Energy (π^*, π) State. The model that describes the key qualitative features of the (π^*, π) spectroscopy of alternate polyenes[47] is based on the assumption of the existence of a pseudoparity symmetry operator. For pyrimidine, this predicts that there should be a pair of A_1 states and a pair of B_2 states, where one member of each of the pairs is forbidden and the other is very intense. This description is formally correct for benzene and metalloporphyrins because for these molecules actual symmetry operators exist that confer these spectroscopic properties. For pyrimidine, two weak bands ($(2)^1A_1$ and $^1B_2$) and two strong bands ($(3)^1A_1$ and $(2)^1B_2$) are expected, and indeed this is what is observed.[1,17,48] Physically, this result is expected because the model predicts that the four bands comprise not single-determinant excitations involving the highest and second-highest occupied π orbitals and the lowest and second-lowest unoccupied π^* orbitals but rather equally weighted linear combinations of pairs of them. Our calculations indicate that, at all geometries considered, the singlet (π^*, π) states of pyrimidine are properly described as two-determinant excitations. At the geometry of the ground state, this is also found for the triplet (π^*, π) states, but geometry optimization of $^3A_1$ is found to lead to localization into two single-determinant excitations, each with a different preferred geometry. This is illustrated in Figure 2 , where the energy of $^3A_1$ evaluated using EOM-CCSD is plotted against the projected displacement from the ground state in mode 8a. Two localized wells separated by a transition state result; these wells are named $(\alpha)^3A_1$ and $(\beta)^3A_1$, and each corresponds to a single-determinant excitation. The appearance of a double-well surface indicates that the pseudoparity operator is ineffective, and the usual alternate-polyene spectroscopic model is therefore invalid for the triplet states. A similar result has also been obtained for pyridine.[3]

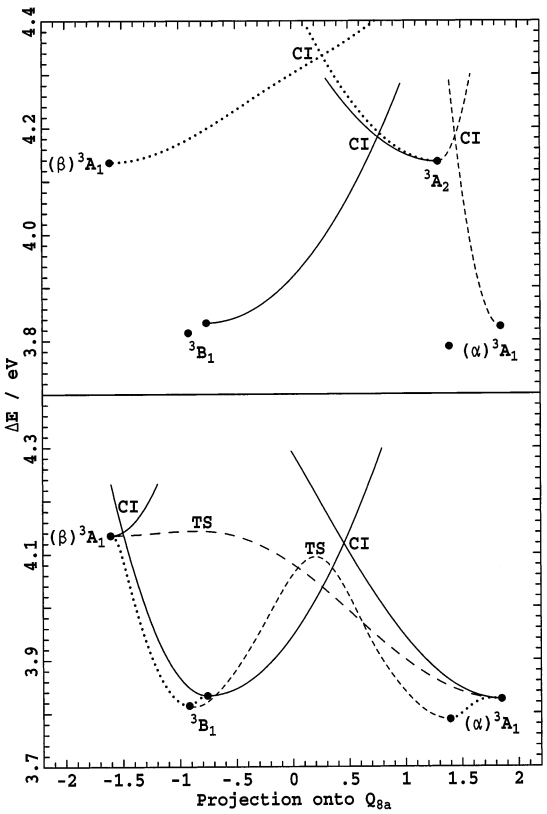

Figure 2. EOM-CCSD maps of the lowest triplet manifold of pyrimidine obtained along linear transits between the $^3B_1$ (both in C_{2v} and C_s symmetry), $(\alpha)^3A_1$ (both in C_{2v} and C_s symmetry), $(\beta)^3A_1$ (C_{2v} symmetry), and $^3A_2$ (C_{2v} symmetry) stationary points (●). The energies are shown as a function of the projection of the displacement from the ground-state equilibrium geometry onto the totally symmetric dimensionless normal coordinate of mode 8a; the approximate location and upper bounds for the energy of various connecting transition states (TS) and conical intersections (CI) are indicated. Within the upper and lower maps, a different dash pattern is used for each pair of state energies evaluated along the same transit.

The calculated reorganization energies display an anomaly in that those for $(\alpha)^3A_1$ and $(\beta)^3A_1$ obtained using CCSD (0.77 and 0.44 eV, respectively) are much larger than those obtained using its time-dependent counterpart, EOM-CCSD (0.45 and 0.15 eV, respectively). This arises because[3] CCSD is essentially

TABLE 5: Observed Vibrational Frequencies for Valence States Other Than $^1B_1$ and $^3B_1$ Compared to Calculated Frequencies ν (cm^{-1}) and Dimensionless Displacements δ[a]

	obsd[b]		EOM-CCSD			CASSCF[c]			CIS		
state	assignment	ν	mode	ν	δ	mode	ν	δ	mode	ν	δ
$^1B_2$	1	950	1	956	1.4	1	979	1.6	1	1053	1.2
	8b	1600	8b	1553					8b	1814	
$(2)^1A_1$	?	770	6a	565	1.5	6a	576	2.3	6a	629	−1.2
			1, 9a, 12	887	0.6	1	906	2.4	9a, 12	952	0.9
			1, 9a, 12	940	1.5	12	979	0.3	1	1028	−1.3
			8a	1688	1.3	8a	1810	1.5	8a	1650	−0.9
$(3)^1A_1$	?	910				1, 9a	977	1.4	1	1023	−1.5
						1, 12	997	0.9	6a	687	0.1
						9a, 12	1129	0.7	9a,12	1073	−0.3
$(2)^1B_2$	?	910	1	921	1.3				1, 9a, 12	998	−0.9
			12	972	1				1, 12	1045	−1.3
			9a	1076	0.8				9a, 12	1164	−0.8

[a] Only specific asymmetric modes and a_1 modes with large displacements are shown. [b] From ref 1. [c] Only a_1 modes are available.

a single-reference method, and such methods typically overestimate the energies of two-determinant states such as $^3A_1$ at the ground-state geometry. Because relaxation results in single-determinant states whose energy is not similarly overestimated, the calculated reorganization energies are too large. Similar results are also obtained when comparing B3LYP and TD-B3LYP results for analogous states.[3] Methods such as CCSD and B3LYP may be very useful, however, as in this circumstance they provide diabatic rather than adiabatic states and hence yield direct information concerning vibronic coupling that is otherwise quite difficult to obtain.[3]

4. Revised Experimental Assignments for Some High-Lying States

The experimental band assignments for the singlet states are firmly grounded on experimental evidence and are, in general, well supported by the computations; one modification is suggested, however. This concerns $(2)^1A_1$, a medium-intensity band sandwiched between the weak $(2)^1B_1$ and strong $(3)^1A_1$/$(2)^1B_2$ band systems.[48] A clear vibrational band is observed at 6.49 eV and is followed to higher energy by a resolved vibrational progression with a spacing of about 0.09 eV (730 cm^{-1}), with poorly resolved features also found at the lower energies of 6.10, 6.26, and 6.38 eV. Bolovinos et al.[48] assigned the 6.49-eV band as the origin of $(2)^1A_1$, with the lower-energy lines possibly accounted for as vibronically intensified transitions of $(2)^1B_1$. However, this assignment attributes a reorganization energy of 0.21 eV to this state, only half of the value predicted by EOM-CCSD. Furthermore, the relative intensities of the bands in the 730-cm^{-1} progression cannot be reconciled using Franck−Condon factor analysis. Our calculations suggest that it is in fact the 6.26-eV line that is the band origin of $(2)^1A_1$. The vibrational modes with the largest calculated displacements are shown in Table 5, but because a variety of modes have similar displacements and frequencies, these calculations predict a complex structure rather than a simple progression in one mode only. We have simulated the low-resolution band structure expected from the EOM-CCSD calculated frequencies, displacements, and Duschinsky matrices, and this is in qualitative agreement with the observed spectra assuming that the origin is located at 6.26 eV; for reference, the observed and simulated spectra are provided in Supporting Information.

All observed vibrational modes for valence excited states[1] other than $^1B_1$ and $^3B_1$ are also shown in Table 5, along with the corresponding calculated vibrational frequencies and displacements. The vibrational assignments[1] for $^1B_2$ are clearly vindicated, although it appears that for the intense overlapping states $(3)^1A_1$ and $(2)^1B_2$ whose vibrational structure is very complex[48] a variety of totally symmetric vibrations are expected to form progressions and no clear interpretation of the apparent progression in 910 cm^{-1} is obtained.

For the triplet states, the assignment of the lowest band as $^3B_1$ is clear from experimental data,[1] but the assignments of the other triplet states arise from the interpretation by Palmer et al.[17] of their low-resolution electron-energy loss spectra obtained by considering multireference configuration interaction (MRCI) calculated vertical excitation energies. Our computational methods place $(\alpha)^3A_1$ and $^3B_1$ close in energy, but the experimental assignment for the lowest state (in benzene crystal at 1.2 K) is most readily confirmed by considering the observed excess atomic spin densities,[49] which B3LYP calculations clearly identify as being those expected for $^3B_1$ rather than any other possible candidate; see Supporting Information.

Modern computational methods are considerably more reliable than the MRCI implementation used in the original assignment by Palmer et al.[17] of the remaining triplet states. Combined with the use of relaxation-energy and singlet−triplet splitting data, they suggest quite different assignments for the high-lying triplet states. Also, our calculations permit the assignment of observed features[17] not originally interpreted; this assignment is shown graphically in Supporting Information. The shoulder observed[17] near 3.6 eV was assigned to $^3B_1$, but because the origin of this band is at 3.54 eV and the calculated reorganization energies exceed 0.3 eV, the band center is clearly being obscured by the strong adjacent excitation. In later discussions, we assume that the band center is at 3.9 eV. The adjacent excitation itself is poorly resolved and may arise from an unresolved state at 4.0 eV, though a clear shoulder is observed at 4.2 eV. We assign the 4.2-eV shoulder to $^3A_2$ on the basis of the calculated singlet−triplet splitting from the known $^1A_2$ state energy (4.6 eV[45]) as well as the calculated and apparent reorganization energies. If a band is indeed present at 4.0 eV, then it could arise from $^3A_1$ and/or $^1B_1$ obscured by $^3A_2$. Palmer et al.[17] assigned a shoulder at 4.5 eV to $^3A_2$ and another at 4.7 eV to $^1A_2$, but because there is a singlet state at 4.6 eV, we assign the 4.7-eV shoulder to $^3B_2$. This value is somewhat lower in energy than the original assignment to a peak at 5.0 eV. We assign the 5.0-eV peak to $(2)^3B_1$ instead and the nearby unassigned 5.3-eV peak to $(2)^3A_2$. An unassigned shoulder at 5.6 eV we attribute to $(2)^3B_1$. All of these assignments should be considered to be provisional; however, because the experimental spectrum is noisy, its structure is poorly resolved, and only computed information is available to use in making the assignments.

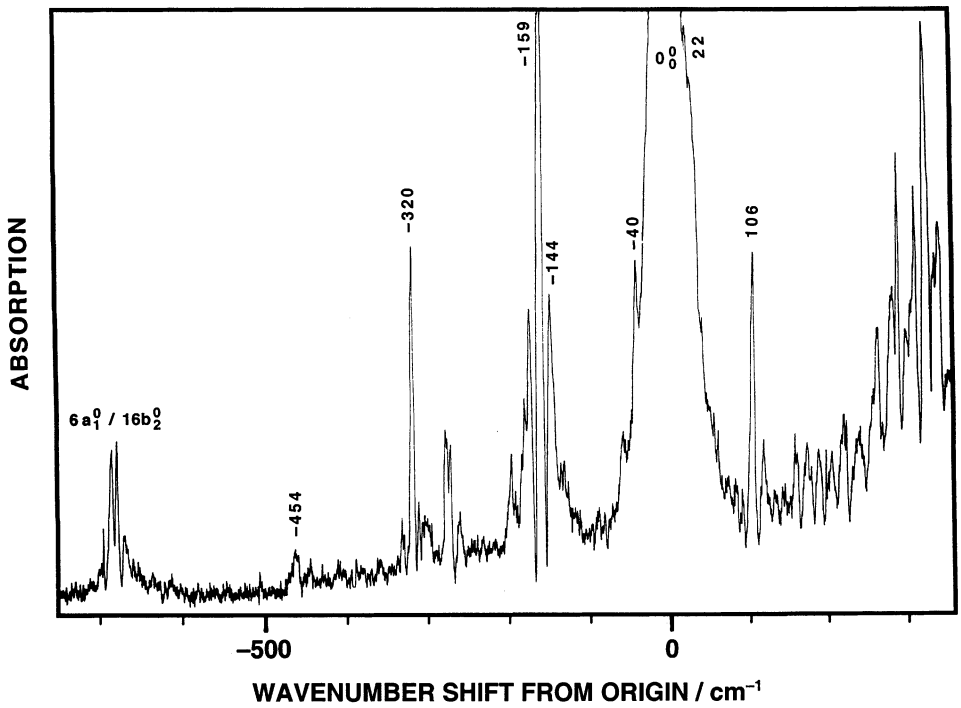

Figure 3. Vapor absorption spectrum of pyrimidine-h_4 at 18 °C in the region of the $^1B_1$ singlet−singlet hot bands.

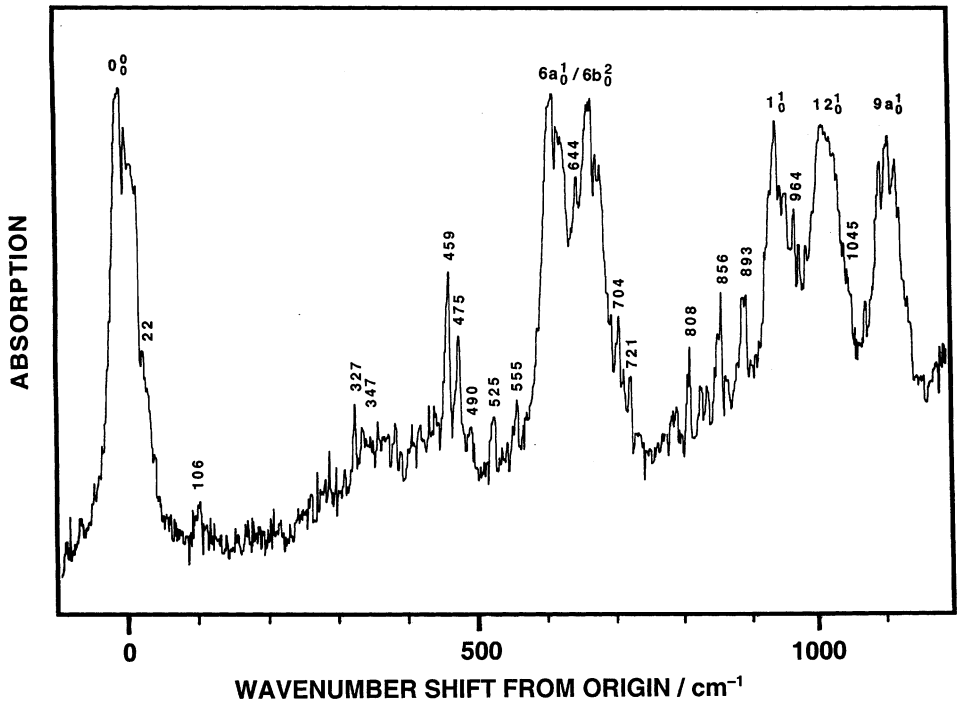

Figure 4. Vapor absorption spectrum of pyrimidine-h_4 at 18 °C; first 1100 cm^{-1} of the $^1B_1$ singlet−singlet system.

5. Spectra, Vibrational Assignments, and Vibronic Coupling for $^1B_1$ and $^3B_1$

The hot-band region of the $^1B_1 \leftarrow {}^1A_1$ ($S_1 \leftarrow S_0$) singlet−singlet absorption spectrum of pyrimidine at 18 °C is shown in Figure 3 whereas the corresponding absorption beyond the origin is shown in Figure 4; the hot-band region of the $^3B_1 \leftarrow {}^1A_1$ ($T_1 \leftarrow S_0$) singlet−triplet spectrum at 75 °C is shown in Figure 5. Analysis of the singlet−triplet spectrum is hampered by the presence of singlet−singlet hot bands; the $^1B_1 \leftarrow {}^1A_1$ origin is only 2542.5 cm^{-1} away,[1] and at 75 °C, the two band systems have comparable intensities in this spectral region. The situation is simpler for pyrazine and pyridazine, for which the singlet−singlet origins are over 4000 cm^{-1} away, and the associated hot bands are much weaker near the singlet−triplet origin. The singlet−singlet and singlet−triplet bands have very similar rotational profiles and cannot be easily distinguished on that basis. A reliable analysis of the $T_1 \leftarrow S_0$ spectrum hinges on a comprehensive knowledge of the $S_1 \leftarrow S_0$ hot bands in this region; fortunately, the singlet−singlet spectrum is well understood, although we suggest some reassignments within it. Our deduced excited-state vibrational frequencies, along with previously known assignments,[20,24] are given in Tables 6 and 7 for the fundamental vibrations of $^1B_1$ and $^3B_1$, respectively, and overtone assignments are given for some significant modes in

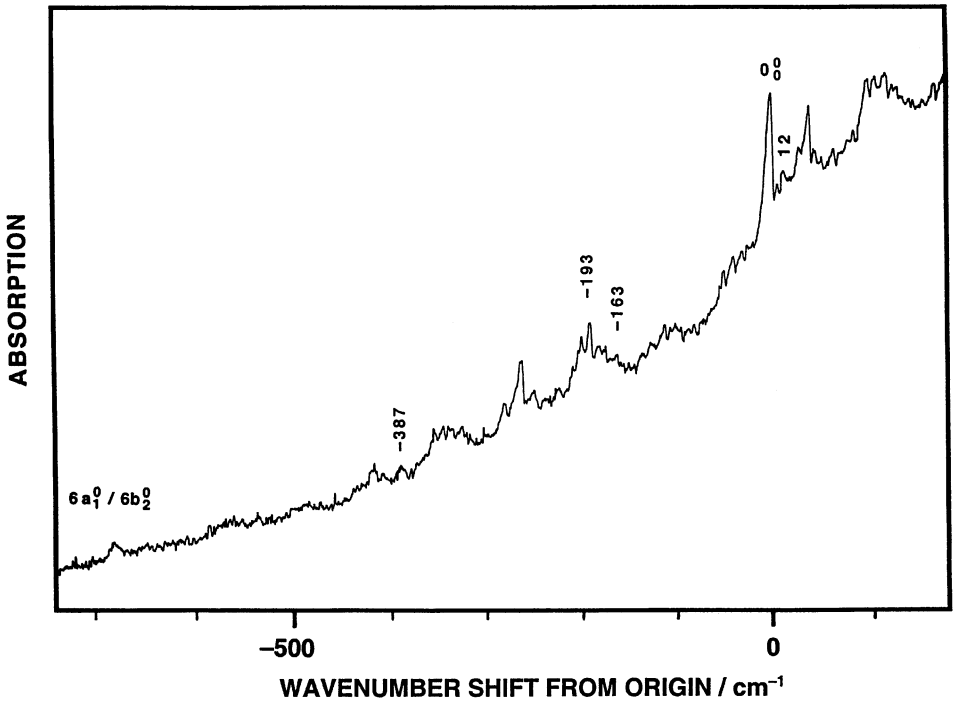

Figure 5. Vapor absorption spectrum of pyrimidine-h_4 at 75 °C (path length 312 m) in the region of the $^3B_1$ singlet−triplet absorption.

TABLE 6: Observed and Calculated Harmonic Vibrational Frequencies[a] (cm^{-1}) for the S_0 and S_1 States of Pyrimidine-h_4 and Pyrimidine-d_4

			ν_1^0 for S_0 ($^1A_1$)			ν_0^1 for S_1 ($^1B_1$)					ν_1^1 for $S_1 \leftarrow S_0$		
mode	sym.	isot.	obsd[b]	CCSD	B3LYP	obsd[f]	EOM-CCSD[a]	CIS[c]	CASPT2	TD-B3LYP[a]	obsd[f]	EOM-CCSD	TD-B3LYP
9a	a_1	h_4	1139	1119	1114	1109[h]	1129	1086	1115	1111	−30	10	−3
		d_4	860	841	843	816[h]	843	818	837	824	−44	2	−19
12	a_1	h_4	1065	1034	1040	1012[h]	1046	998	1030	1030	−53	12	−10
		d_4	1043	1011	1019	1003[h]	1012	967	937	1005	−42	1	−14
1	a_1	h_4	992	968	972	941[h]	958	928	936	945	−51	−10	−27
		d_4	975	953	958	929[h]	951	918	928	934	−46	−2	−24
6a	a_1	h_4	678	689	692	625[d]	652	628	637	641	−53[d]	−37	−51
		d_4	657	667	669	604[d,h]	628	607	615	619	−53[d]	−39	−50
6b	b_2	h_4	623	629	631	329	76i	335	312	377i	−294[g]	x[i]	x[i]
		d_4	603	610	611	300	74i	328	299	367i	−303[g]	x[i]	x[i]
11[e]	b_1	h_4	960	982	980	915	949	902		914	−40[g]	−33	−66
10b	b_1	h_4	811	824	824	612	656	655		629	−199[g]	−168	−195
4	b_1	h_4	721	738	739	444	471	465		460	−277[g]	−267	−279
		d_4	553	569	564	369	380	390		378	−184[g]	−189	−186
16b	b_1	h_4	344	360	354	366	380	388		363	22[h]	20	9
		d_4	304	312	305		328	332		311	<10	16	6
16a	a_2	h_4	399	410	409	240	254	290	200	253	−159[h]	−156	−156
		d_4	369	378	374	237	236	274	188	239	−136[h]	−142	−135
17a	a_2	h_4	980	960	959	526	544	556	471	560	−454[g]	−416	−399
		d_4	801	777	778	424	439	447	375	444	−377[g]	−338	−334
RMS error		h_4		20	19		28	28		15		35	23
		d_4		16	12		22	24		23		29	25

[a] i indicates imaginary frequencies. [b] From refs 1, 31, and 32. [c] Scaled by 0.89. [d] Fermi resonance-corrected. [e] Sometimes[1] listed as 17b. [f] Directly observed quantity is ν_0^1 for the a_1 modes and ν_1^1 otherwise; $\nu_1^1 = \nu_0^1 - \nu_1^0$. [g] This work. [h] From refs 18 and 31. [i] Not available because the frequency is imaginary for S_1.

Table 8. For comparison, computed harmonic vibrational frequencies are provided in Tables 6 and 7, and these, as corrected for diagonal anharmonicity, are provided in Table 8. Vibrational frequency changes between the ground and excited states, ν_1^1 and so forth, are also provided in these Tables for the purpose of analyzing sequence bands. Detailed assignments of the singlet−singlet and singlet−triplet spectra are provided in Tables 9 and 10, respectively.

The hot bands and sequence structure in the absorption spectrum are expected to arise from the lowest-frequency modes in the ground state, owing to their more favorable Boltzmann factors. As shown in Tables 6 and 7, these are, in order of

TABLE 7: Observed and Calculated Harmonic Vibrational Frequencies (cm^{-1}) for the S_0 and T_1 States of Pyrimidine-h_4

		ν_1^0 for S_0 ($^1A_1$)			ν_0^1 for T_1 ($^3B_1$)					ν_1^1 for $T_1 \leftarrow S_0$		
mode	sym.	obsd[d]	CCSD	B3LYP	obsd[e]	EOM-CCSD	CIS[b]	CASPT2	B3LYP	obsd[e]	EOM-CCSD	B3LYP
9a	a_1	1139	1119	1114	1082[f]	1128	1082	1116	1114	−57	9	0
12	a_1	1065	1034	1040	1007[g]	1044	995	1030	1029	−58	11	−11
1	a_1	992	968	972	941[g]	963	935	946	956	−51	−5	−16
6a	a_1	678	689	692	616[c]	650	620	636	652	−62	−39	−40
6b	b_2	623	629	631	319	412	278	571	437	−304[g]	−217	−194
11[a]	b_1	960	982	980		939	935		898		−43	−82
10b	b_1	811	824	824	648	626	784		619	−163[g]	−198	−205
4	b_1	721	738	739		298i	620		238			−501
16b	b_1	344	360	354	356	396	403		431	12[g]	36	77
16a	a_2	399	410	408	206	282	310	537	288	−193[g]	−128	−120
17a	a_2	980	960	959		517	522	805	487		−443	−472
RMS error			20	19		56	62	73	65			

[a] Sometimes[1] listed as 17b. [b] Scaled by 0.89. [c] Fermi resonance-corrected. [d] From ref 32. [e] Directly observed quantity is ν_0^1 for the a_1 modes and ν_1^1 otherwise; $\nu_1^1 = \nu_0^1 - \nu_1^0$. [f] From ref 24. [g] This work.

TABLE 8: Comparison of Experimental and EOM-CCSD and B3LYP Anharmonic Frequencies (cm^{-1}) for Selected Modes of Pyrimidine and Pyrimidine-d_4[a]

			S_0 ($^1A_1$)			S_1 ($^1B_1$)					T_1 ($^3B_1$)				
mode	sym.	method	ν_1^0	ν_2^0	$\nu_2^0 - 2\nu_1^0$	ν_0^1	ν_0^2	$\nu_0^2 - 2\nu_0^1$	ν_1^1	ν_2^2	ν_0^1	ν_0^2	$\nu_0^2 - 2\nu_0^1$	ν_1^1	ν_2^2
6b	b_2	obsd	623[d]	1240[e]	−6	329	657[b]	−1	−294[g]	−583	319	612[b]	−26	−304[g]	−628
$-h_4$		CCSD[c]	631	1262	2	371	846	104	−259	−415	420	848	8	−211	−413
		B3LYP[c]	633	1267	1	493	1148	162	−140	−119	444	894	6	−189	−373
4	b_1	obsd	721[d]			444	893[g]	5	−277[g]						
$-h_4$		CCSD[c]	743	1491	6	493	1006	20	−250	−484	174	473	125	−568	−1017
		B3LYP[c]	747	1500	6	485	994	24	−262	−506	294	628	40	−453	−872
16b	b_1	obsd	344[d]	682[b,g]	−6	366	788	56	22[e]	106[g]	356			12[g]	
$-h_4$		CCSD[c]	368	743	7	394	800	12	26	57	407	824	10	39	97
		B3LYP[c]	363	735	9	389	802	24	26	67	437	880	6	74	145
16b	b_1	obsd	304[d]	609[f]	1	∼304−314	674	66−46	<10	65[f]					
$-d_4$		CCSD[c]	318	643	7	343	701	15	25	58					
		B3LYP[c]	312	630	6	338	720	44	26	90					
16a	a_2	obsd	399[d]	810[h]	12	240	490[g]	10	−159[g]	−320[g]	206	418	6	−193[g]	−387[g]
$-h_4$		CCSD[c]	415	836	6	270	554	14	−139	−266	294	598	10	−115	−222
		B3LYP[c]	416	838	6	275	568	18	−141	−270	303	621	15	−113	−217

[a] ν_1^0 is the ground-state vibration frequency; the excited-state frequency ν_0^1 is obtained experimentally as $\nu_1^0 + \nu_1^1$. [b] Corrected for Fermi resonance. [c] TD-B3LYP or EOM-CCSD for S_1. [d] From ref 32. [e] From ref 18. [f] From ref 30 . [g] This work. [h] Obtained using $\nu_2^0 = \nu_0^2 + \nu_2^2$.

increasing frequency,[32] 16b (b_1, experimental value for the ground state (344 cm^{-1})), 16a (a_2, 399 cm^{-1}), 6b (b_2, 623 cm^{-1}), 6a (a_1, 678 cm^{-1}), 4 (b_1, 721 cm^{-1}), 10b (b_1, 811 cm^{-1}), 11 (b_1, 960 cm^{-1}), 17a (a_2, 980 cm^{-1}), and 1 (a_1, 992 cm^{-1}).

5A. Untangling the $6a_0^1/6b_0^2$ Fermi Resonance. Fermi resonances between mode 6a and the first overtone of mode 6b are typical of diazine absorption spectra and are associated with the halved frequency of mode 6b in the excited state. This reduction in frequency is attributed to strong vibronic coupling between the closely spaced B_1 and A_2 states, and we address the chemical significance of this coupling in the next subsection. In the singlet−triplet spectrum, the $6a_0^1/6b_0^2$ Fermi doublet occurs at 599/628 cm^{-1}; Ottinger et al.[24] also reported these bands in their phosphorescence excitation spectrum but did not identify them as a Fermi doublet. One of the major features of the singlet−singlet spectrum shown in Figure 4, first reported by Knight et al.,[18] is the corresponding doublet that occurs at 613/669 cm^{-1}. The intensity ratios are quite different for the two spectra: in the singlet−singlet spectrum, the components of the doublet have similar intensities, but in the singlet−triplet spectrum, the bands at 599 and 628 cm^{-1} have an intensity ratio of about 1:4.[24]

The different intensity ratios may be satisfactorily modeled by anharmonic coupling calculations. Before Fermi resonance, both the $6a_0^1$ and $6b_0^2$ modes have intrinsic intensity due to the displacement in mode 6a and the large frequency change in mode 6b, and we calculate Franck−Condon factors for these using calculated displacements (see Supporting Information) and approximate observed frequencies, respectively. Hence, for the singlet−singlet spectrum, a coupling constant of 21 cm^{-1} and a zeroth-order separation of 32 cm^{-1}, placing $6b_0^2$ at 657 cm^{-1} and $6a_0^1$ at 625 cm^{-1}, give a close approximation to the observed intensity ratio and doublet splitting. In the singlet−triplet spectrum, the ratio and splitting were successfully modeled using a coupling constant of 15 cm^{-1} and separation of 4 cm^{-1}, placing $6b_0^2$ at 612 cm^{-1} and $6a_0^1$ at 616 cm^{-1}. The different intensities for the two spectra are due to the different pattern of constructive and destructive interference that occur with the reversed ordering of the zeroth-order levels.

Further confirmation of the Fermi-resonance analysis could be provided by $6a_1^1$, but unfortunately, this sequence band is not clearly identified in either the singlet−singlet or singlet−triplet spectra. This is surprising because, on the basis of the calculated vibrational displacements provided in Supporting Information, the Franck−Condon factor for $6a_1^1$ is expected to be slightly larger than that for $6a_1^0$ and there are clear $16b_2^0/6a_1^0$ Fermi doublets observed at −678 and −685 cm^{-1} in both spectra. (See Figure 4, Tables 9 and 10, and the study by Knight et al.[18]) Unfortunately, the consequence of the interplay of the

TABLE 9: Band Assignments for the Origin Regions of the $^1B_1 \leftarrow {}^1A_1$ (π^*, n) Band Systems of the Vapor Absorption Spectrum of Pyrimidine-h_4 and Pyrimidine-d_4

pyrimidine-d_4		pyrimidine-h_4			
$\nu - 31\,188$ cm^{-1}	assignment	$\nu - 31\,073$ cm^{-1}	assignment	$\nu - 31\,073$ cm^{-1}	assignment
−658	$6a_1^0$	−685	$6a_1^0/16b_2^0$	347	$6a_0^1/6b_0^2\,16a_2^2$
		−678	$6a_1^0/16b_2^0$	459	$6a_0^1/6b_0^2\,16a_1^1$
−377	$17a_1^1$	−454	$17a_1^1$	475	
−270	$16a_2^2$	−320	$16a_2^2$	490	$16a_0^2$
−303	$?6b_1^1$	−294	$?\,6b_1^1$	525	$6a_0^1/6b_0^2\,16a_1^1$
−236				555	
−184	4_1^1	−277	4_1^1	613	$6a_0^1/6b_0^2$
		−199	$10b_1^1$	644	$6a_0^1/6b_0^2\,16b_1^1$
		−174		669	$6a_0^1/6b_0^2$
−136	$16a_1^1$	−159	$16a_1^1$	704	$6a_0^1/6b_0^2\,16b_1^1$
		−144	$16a_1^1 16b_1^1$	721	
		−57?	$16a_1^1 16b_2^2$	788	$1_0^1 16a_1^1$
		−40	11_1^1	808	
0	S_1 origin	0	S_1 origin	856	$12_0^1 16a_1^1$
		22	$16b_1^1$	893	4_0^2
65	$16b_2^2$	106	$16b_2^2$	941	1_0^1
		255	$1_0^1 6a_1^0/16b_2^0$	965	$1_0^1 16b_1^1$
		286	$6a_0^1/6b_0^2\,16a_2^2$	1012	12_0^1
		327	$6a_1^0/16b_2^0\,12_0^1$	1045	$12_0^1 16b_1^1$

TABLE 10: Band Assignments for the $^3B_1 \leftarrow {}^1A_1$ (π^*, n) Band System of the Vapor Absorption Spectrum of Pyrimidine-h_4

$\bar{\nu} - 28\,534$ cm^{-1}	assignment	$\bar{\nu} - 28\,534$ cm^{-1}	assignment
−685	$6a_1^0/16b_2^0$	406	$6a_0^1/6b_0^2\,16a_1^1$
−678	$6a_1^0/16b_2^0$	442	$6a_0^1/6b_0^2\,16a_1^1$
		599	$6a_0^1/6b_0^2$
−538	?	628	$6a_0^1/6b_0^2$
−418	?		
−387	$16a_2^2$	640	$6a_0^1/6b_0^2\,16b_1^1$
−304	$6b_1^1$	813	$12_0^1 16a_1^1$
−193	$16a_1^1$	906	$?\,1_0^1$
−163	$?10b_1^1$	941	$?\,1_0^1$
0	T_1 origin	1007	12_0^1
12	$16b_1^1$	1019	$S_1\,6a_2^0\,16a_1^1$
365	?		

$6a_0^1/6b_0^2$ Fermi resonance in the excited state and the well-known $6a_1^0/16b_2^0$ Fermi resonance in the ground state is that $6a_1^1$ is actually expected to appear not as a single line but rather as a quartet, making it difficult to identify. In the singlet−triplet spectrum, three unassigned peaks are observed in the region of −63 cm^{-1}, naively expected for $6a_1^1$: these are at −52, −82, and −89 cm^{-1}. Also, the similarity between the two sets of $16b_2^0/6a_1^0$ Fermi doublets strongly confirms our assignment of the singlet−triplet origin, which is in agreement with earlier deductions.[24]

5B. B_1-A_2 Vibronic Coupling through Mode 6b: Possible (π^*, n) Symmetry Breaking. The large depression observed in the frequency of mode 6b (b_2) in the B_1 excited states (see section 5A) is due to vibronic coupling with states of A_2 symmetry. Experimentally, the $^1A_2$ and $^3A_2$ states are located vertically about 0.5 and 0.6 eV above the corresponding B_1 states, respectively. Our calculations predict that both $^1A_2$ and $^3A_2$ experience strong vibronic coupling in b_1 modes with the ca. 0.4-eV higher B_2 states and undergo out-of-plane distortion. They also predict that the reorganization energies for the A_2 states are ca. 0.3 eV larger than those for the B_1 states, and hence one would expect the adiabatic energy gaps to decrease to about 0.2−0.3 eV. Specifically, the CCSD, EOM-CCSD, and B3LYP calculations predict the vertical energy gap between $^3B_1$ and $^3A_2$ to within 0.1 eV of experiment and a 0−0 energy difference of 0.2−0.3 eV. The EOM-CCSD result is shown on the lowest-triplet manifold map in Figure 2 along with the approximate locations and energies for the conical intersections involving $^3B_1$ and $^3A_2$. These results indicate that $^3A_2$ will be significant in relaxation processes on this manifold.

EOM-CCSD predicts that the A_2-B_1 gap is reduced by 0.2 eV in the singlet manifold compared to that in the triplet and hence predicts that the $^1B_1$ and $^1A_2$ origins are nearly degenerate. The observed high-resolution spectrum of $^1B_1$ shows no indication of an additional origin within 0.2 eV, however. By linear interpolation between the minima of $^1B_1$ and $^1A_2$, we have obtained an approximate geometry (see Table 1) and EOM-CCSD energy upper bound of 0.20 eV above the origin of $^1B_1$ for the conical intersection between these two states. This is in the Franck−Condon region, and hence we would expect that if $^1A_2$ is located as close as EOM-CCSD predicts then significant perturbations to the spectrum of $^1B_1$ would indeed occur. However, EOM-CCSD(T) calculations[10] also suggest that EOM-CCSD underestimates the $^1B_1$ to $^1A_2$ gap by 0.2 eV; adjusting the EOM-CCSD CI energy by this amount would take the CI out of the Franck−Condon region, making the detection of $^1A_2$ more difficult.

The naive interpretation of the observed similar frequency lowerings (see Table 8) in the singlet and triplet states is that the vibronic coupling and hence the singlet and triplet energy gaps are actually very similar, as suggested by EOM-CCSD-(T). The shapes of the calculated potential energy surfaces, and hence computed vibrational frequencies, are very sensitive to the calculated energy gaps, with the consequence that EOM-CCSD predicts that $^1B_1$ has a double-well potential in mode 6b, the well depth being just 0.2 cm^{-1} (see Supporting

Information) whereas no such distortion is predicted for $^3B_1$. We have evaluated the EOM-CCSD(T) energy along the normal coordinate for mode 6b of $^1B_1$ and have found only a single well, a result that is consistent with the larger interstate gap predicted by this method. CASPT2 also predicts that $^1B_1$ is stable to b_2 distortion whereas TD-B3LYP predicts a shallow double well.

Quantitative experimental evidence for the nature of the vibronic coupling through mode 6b can come from observed vibrational anharmonicities. In the singlet−triplet spectrum, the sequence band $6b_1^1$ associated with the third-lowest ground-state frequency is tentatively assigned to a weak band at −304 cm^{-1}, suggesting that $6b_0^1$ should be found at 319 cm^{-1}; the corresponding singlet−singlet sequence band occurs at −294 cm^{-1}, suggesting 329 cm^{-1} for $6b_0^1$. Hence, after Fermi-resonance correction of the frequencies of $6b_0^2$, we see in Table 8 that 6b appears to be quite harmonic in the ground and S_1 states (the anharmonicities $6b_0^2 - (2 \times 6b_0^1)$ are −6 and −1 cm^{-1}, respectively) whereas T_1 displays an anharmonicity of −26 cm^{-1}. For S_1, the EOM-CCSD and TD-B3LYP calculations predict double-well potential energy surfaces with very shallow well depths of 0.2 and 15 cm^{-1}, respectively. Surprisingly, these methods actually overestimate the observed frequency $6b_0^1$ by 50−150 cm^{-1}. Nevertheless, the predicted large positive anharmonicities, which are a significant qualitative feature of double-well surfaces, are not supported by the experimental data. It is thus apparent that EOM-CCSD and TD-B3LYP overestimate the strength of the vibronic coupling between the $^1B_1$ and $^1A_2$ states, a result that is not surprising given that these methods underestimate the energy gap between the states.

Possible distortions in b_2 modes such as 6b for pyrimidine are chemically very significant because they serve to localize the (π^*, n) excitation on one of the two nitrogen atoms rather than delocalizing it over both. For pyrimidine, the excitation is clearly delocalized in both the lowest singlet and triplet excited states. This result is analogous to that found for pyrazine,[50] though for this molecule the belief that the (π^*, n) excitation must be localized led to a history of incorrect assignments of the spectroscopic transitions.[16,50,51]

5C. Modes 16a and 17a: Vibronic Coupling to B_2 States. Because of a reasonably large Boltzmann factor, the $16a_1^1$ sequence is expected to be relatively strong, and we assign it to the singlet−triplet sequence band at −193 cm^{-1}. This sequence is also seen on the $6b_0^2/6a_0^1$ Fermi doublet, and all corresponding bands are discernible in the phosphorescence-excitation spectrum.[24] The band at −387 cm^{-1} (2×193.5 cm^{-1}) may be assigned to $16a_2^2$, suggesting that this mode behaves harmonically; this conclusion is supported by the calculations shown in Table 8. The corresponding $16a_1^1$ singlet−singlet sequence occurs at −159 cm^{-1}, so the mode has frequencies of 240 and 206 cm^{-1} in the S_1 and T_1 states, respectively, compared to 399 cm^{-1} in the ground state.

Mode 17a is of much higher frequency in the ground state and hence is more difficult to observe in sequence bands. Deuteration lowers the ground-state frequency considerably, however, and from the available[31] high-resolution singlet−singlet spectrum of pyrimidine-d_4, we assign a sequence band at −377 cm^{-1} to $17a_1^1$. On the basis of this, the assignment of a weak line at −454 cm^{-1} in the spectrum of pyrimidine-h_4 to $17a_1^1$ is suggested. These assignments are strongly supported by the calculations because they predict that significant vibronic activity in mode 17a dramatically reduces the excited-state frequency and discount previous[31] assignments of 17a at 927 cm^{-1}. A possible alternative assignment of the −454 cm^{-1} line is $16a_3^3$, which on the basis of the observed frequencies for $16a_1^1$ and $16a_2^2$ is expected, with somewhat less intensity, at −468 cm^{-1}; this assignment is rejected because the implied degree and nature of the anharmonicity for 16a cannot readily be justified.

Qualitatively, the computational methods all reproduce the observed 130−450 cm^{-1} lowerings of the frequencies of the two a_2 modes in the lowest B_1 excited states. These changes are indicative of strong vibronic coupling between the lower B_1 and B_2 states. Quantitatively, there are some significant differences, however. For $^1B_1$, all methods calculate the changes in mode 16a to within 20 cm^{-1}, an excellent result, whereas for $^3B_1$, EOM-CCSD underestimates the lowering by 65 cm^{-1} and B3LYP underestimates it by 73 cm^{-1} (see Table 8). The experimentally observed enhanced lowering of 16a for $^3B_1$ suggests that the B_1/B_2 energy gap is smaller in the triplet manifold. Although the original assignments of the EEL spectra indicated that this gap increases by 0.45 eV, our revised assignments given in Table 2 embody a 0.2-eV reduction that is consistent with the vibronic-coupling analysis. Furthermore, the lowering predicted by B3LYP in the triplet state appears to be related to the exaggerated decrease of the B_1/B_2 gap of 0.5 eV predicted by B3LYP (see Table 2) whereas the understated depression predicted by EOM-CCSD appears to be related to its failure to modify this gap. Clearly, the ability of computational methods to treat vibronic coupling is strongly linked to their ability to calculate accurate excited-state energy differences.

5D. Mode 16b: Vibronic Coupling to the Ground State. Owing to a favorable Boltzmann factor, the $16b_1^1$ sequence band should be relatively strong, and we tentatively assign it to a weak band at $0_0^0 + 12$ cm^{-1} in the singlet−triplet spectrum. A weak band seen at 12 cm^{-1} to the blue of the higher-energy component of the $6b_0^2/6a_0^1$ Fermi doublet is similarly assigned to the associated $16b_1^1$ sequence band; the lower-energy component is significantly weaker, and the sequence band is lost in hot bands of the singlet system, however. These lines are also apparent in the phosphorescence-excitation spectrum of pyrimidine.[24] In the singlet−singlet spectrum, a sequence band is seen at $0_0^0 + 22$ cm^{-1} that has previously[30] been assigned as $6b_1^1$. However, this assignment is refuted by the SVL fluorescence spectra from the Fermi doublets at 613 and 669 cm^{-1} for pyrimidine[18] and at 596 and 646 cm^{-1} for pyrimidine-d_4,[31] which unequivocally show that the frequency of 6b is approximately halved. Alternatively, we assign $0_0^0 + 22$ cm^{-1} as $16b_1^1$, providing a consistent analysis for all spectra.

It is rather unusual that sequence bands such as this should be at higher frequency than the origin, indicating that the vibrational frequency in the excited state is *higher* than that in the ground state. This phenomenon has been observed for mode 16b in pyridazine, however.[13] Strong support for this assignment comes from the results of the EOM-CCSD and B3LYP calculations shown in Tables 6−8 because consistent, sizable vibrational frequency increases are predicted to occur *only* for mode 16b; for the related mode 16a, the calculations predict large frequency decreases, indicating the uniqueness of the behavior of 16b.

Absorptions are also found in the long-path-length singlet−singlet spectrum at +33 and +24 cm^{-1} from the 12_0^1 and 1_0^1 bands, respectively. These we also attribute to $16b_1^1$. The corresponding bands on the $6b_0^2/6a_0^1$ Fermi doublet at 613/669 cm^{-1} occur at +31 and +35 cm^{-1}, and the apparent dependence on the accompanying mode suggests that mode 16b is anhar-

monic. The assignment of the weak band at +106 cm^{-1} (Figure 4) may also be relevant here. Although earlier spectra showed the existence of this band, it had not previously been assigned. Indeed, we have been unable to propose any potential assignments other than $16b_2^2$, which would be satisfactory on intensity grounds. This assignment depicts mode 16b as being strongly anharmonic. Supporting these assignments, the calculations predict values for the excited-state frequency increases that are close to those observed; see Table 8, which gives a value for the $^1B_1$ state of $16b_1^1 = 26$ cm^{-1} by both EOM-CCSD and TD-B3LYP compared to the observed value of 22 cm^{-1}. For $16b_2^2$, the computed values are 57 and 67 cm^{-1}, respectively, compared to 106 cm^{-1}. However, the calculated anharmonicities, $16b_2^2 - (2 \times 16b_1^1)$, are 12 and 24 cm^{-1}, respectively, for the above example, which are not as large as the observed value of 56 cm^{-1}. For pyrimidine-d_4, a line observed at the origin + 65 cm^{-1} has previously[30] been assigned to $16b_1^1$. On the basis of our calculated frequencies, it is much more likely that this line arises from $16b_2^2$ instead, and this reassignment has been made in the Tables. In this scenario, $16b_1^1$ is presumed to lie underneath the intense origin absorption and hence can be no larger than ca. 10 cm^{-1}.

The increase in frequency of mode 16b on excitation is attributed to vibronic coupling between $^1B_1$ and the ground state, $^1A_1$. Such coupling would decrease the frequency of 16b in the ground state and simultaneously increase it in $^1B_1$. As a result, the frequency increase in $^1B_1$ from the ground state is expected to be twice that for $^3B_1$, in agreement with the experimental ratio of 22:12. (See Table 8.) The calculations, however, predict *greater* frequency increases for the triplet state than for the singlet. Although 16b is the lowest-frequency b_1 mode in the ground state, the calculations predict that, as a result of vibronic coupling to the excited $^3A_1$ states, the second-lowest mode, mode 4, is depressed to a frequency lower than that of 16b in $^3B_1$ (see Section 5F) but remains at a higher frequency in $^1B_1$. Duschinsky rotation involving these two modes would lower the frequency of 16b in $^1B_1$ and raise it in $^3B_1$; this scenario would be expected to lead to situations in which the apparent frequency of 16b becomes strongly dependent on resonances and hence the nature of accompanying modes, as is observed. We see that although the calculations are able to isolate the important chemical effects they are not sufficiently accurate to be able to predict these unusual spectroscopic properties a priori.

5E. Other Singlet−Triplet Lines: Possible Assignments for Modes 4, 11, and 10b. Weak bands are observed in the singlet−triplet spectrum at −163 and −538 cm^{-1} that are not readily assigned. These appear to be of singlet−triplet rather than singlet−singlet character. For example, the only other possibility for the −538 cm^{-1} line is the S_1 $6a_3^0/12_1^0$ hot band, but this should be broad because of the Fermi resonance and extremely weak because $6a_2^0/12_1^0$ is quite weak. Another possible candidate for a singlet−triplet sequence band is −418 cm^{-1}, although the singlet−singlet hot band $[6a_1^0/16b_2^0]9a_2^0$ is a serious possibility also. The most likely candidates for additional singlet−triplet sequence bands are 4_1^1, 11_1^1, and $10b_1^1$. On the basis of the calculations, $10b_1^1$ is expected at around −200 cm^{-1}, and so the line at −163 cm^{-1} is tentatively assigned to this transition. However, the presence of hot bands of the singlet system in this region, in particular the $6a_4^0...16b_8^0$ Fermi quintet, needs also to be considered. The EOM-CCSD and B3LYP calculations predict only −43 and −82 cm^{-1} for 11_1^1 (see Table 7), and no assignment for this band can be made. Possible assignments for mode 4 are discussed in section 5F below.

5F. B_1-A_1 Vibronic Coupling via ν_4: Possibility of a Boat Distortion in $^3B_1$. The calculations for most of the excited states reflect the occurrence of strong vibronic coupling in b_1 vibrational modes. Although the nature of the distortion varies considerably between states (see Supporting Information), we focus on the boat distortion shown in Figure 1, which is caused primarily by displacement in mode 4. As shown in Tables 6 and 8, a large frequency reduction of 277 cm^{-1} is observed for this mode in $^1B_1$ compared to the frequency of the ground state. All computational methods predict that this effect is enhanced for $^3B_1$ because the A_1 states, to which the B_1 states couple via b_1 vibrational modes, are predicted to be of much lower energy in the triplet manifold; see Tables 2 and 3. No clear assignment of lines such as 4_1^1 and 4_0^2 is possible for $^3B_1$, although some possibilities are discussed below.

EOM-CCSD correctly predicts that $^1B_1$ has a single-well potential as a function of mode 4, the frequency reduction being accurately reproduced at 267 cm^{-1}. However, EOM-CCSD predicts that $^3B_1$ has a shallow double-well structure and undergoes distortion to $\theta = 15°$, $\phi = 4°$; see Table 1. After distortion, the state is still identifiably $^3B_1$, bearing the primary geometrical (see Table 1) and spin-density (see Supporting Information) signatures of this state. The location and energy of both the C_{2v} and C_s variants of this state are indicated on Figure 2, which is an EOM-CCSD map of the lowest triplet manifold of pyrimidine. The well depth is just 0.019 eV or 150 cm^{-1} (see Table 4), which is insufficient to support zero-point vibration. B3LYP predicts that mode 4 is lowered by 279 cm^{-1} for the singlet state and by 501 cm^{-1} for the triplet, with both surfaces having a single minimum. After anharmonic analysis, the EOM-CCSD frequency for the triplet state (see Table 8) shows a lowering of 568 cm^{-1}.

It is believed that the $^1B_1$ and $^3B_1$ states have similar equilibrium geometries on the basis of the band shapes of the lines in their emission and absorption spectra,[20,24] but this argument cannot differentiate between the qualitatively different potential energy surfaces predicted by the two computational methods. What is required is the precise determination of 4_1^1 and 4_0^2.

The spectra suggest three possibilities for these assignments. First, the observed line at −538 cm^{-1} in the singlet−triplet spectrum could be assigned to 4_1^1, implying a frequency for 4_0^1 of 183 cm^{-1} (calculations: EOM-CCSD 174 cm^{-1}, B3LYP 294 cm^{-1}). If the potential energy surface is a typical single-minimum surface, then anharmonicity should be low, and one would expect to find 4_0^2 near 366 cm^{-1}. Indeed, a weak band at 365 cm^{-1} is observed, though it could also be attributed to a hot band of the singlet−singlet spectrum. This assignment is also unlikely because no band in this region is observed in the phosphorescence-excitation spectrum,[24] and on the basis of Franck−Condon factors, 4_0^2 would naively be expected to be 16% as intense as the origin band. Also, all computational methods predict positive rather than negative anharmonicity for this mode.

The second possible assignment for 4_1^1 is the observed line at −418 cm^{-1}, implying a vibrational frequency of 303 cm^{-1}. This is plausible because this frequency is less than that observed for $^1B_1$, consistent with all computational predictions, and if the vibration is harmonic, then 4_0^2 would be hidden by the large complex signal due to the Fermi doublet $6a_0^1/6b_0^2$.

The third possibility is that the band evident in the phosphorescence-excitation spectrum[24] at about 310 cm^{-1} is due to 4_0^2. In the gas-phase fluorescence spectrum,[18] a line possibly

attributable to 4_2^0 is evident at about 1403 cm^{-1} and has an intensity similar to that expected on the basis of Franck−Condon factors for a frequency change of this order. However, the observed intensity of the line in the phosphorescence-excitation spectrum is only one-quarter of that expected. Calculations performed using the calculated anharmonic potential energy surfaces indicate that the intensity could be halved because of anharmonicity, making this assignment plausible. Indeed, it is difficult to find any assignment other than 4_0^2 for what is a significant feature in the phosphorescence-excitation spectrum. Unfortunately, we are unable to identify clearly any corresponding lines in the singlet−triplet absorption spectrum (in, say, the −570 to −620 cm^{-1} region) that could be assigned to 4_1^1 and hence confirm the assignment. This third possibility would strongly suggest that the EOM-CCSD description of the potential energy surface is realistic and that a shallow double minimum is indeed present in the lowest $^3B_1$ state. Such a scenario is reminiscent of pyridine, for which the analogous distortion is very deep and gives rise to a very complex singlet−triplet spectrum.[3]

5G. Boat Distortion to the $^3A_1$ States and the Nature of the Vibronic Coupling with $^3B_1$. In C_{2v} symmetry, the $(\alpha)^3A_1$ and $(\beta)^3A_1$ states are predicted by both EOM-CCSD and B3LYP computations to be unstable with respect to distortion in mode 4 due to the vibronic coupling with $^3B_1$. These distortions are predicted to be much larger than those previously considered for $^3B_1$, and hence the computed results are likely to provide a realistic description of the nature of these excited states. As shown in Figure 2, quite different qualitative behavior is predicted by EOM-CCSD for the two $^3A_1$ states. The lower-energy state, $(\alpha)^3A_1$, undergoes a large-angle ($\theta = 28°$, $\phi = 21°$) distortion with a well depth of 0.038 eV (300 cm^{-1}) and retains its original character whereas $(\beta)^3A_1$ proceeds without barrier to the C_s structure of $^3B_1$. Hence, we see that the EOM-CCSD calculation ascribes the vibronic coupling of $^3B_1$ via b_1 modes as occurring primarily with the high-energy state $(\beta)^3A_1$ rather than with the low-energy $(\alpha)^3A_1$ state. EOM-CCSD, which appears to overestimate the coupling, predicts a 0.3-eV gap to $(\beta)^3A_1$ whereas B3LYP predicts a gap of 0.5 eV (see Table 3), which appears to be more consistent with the experimental spectra. Errors of this magnitude in the calculated interstate energy differences are quite plausible. Because strong coupling is not predicted to occur between the $^3B_1$ and $(\alpha)^3A_1$, states that are predicted to be nearly degenerate, the lack of perturbation by $(\alpha)^3A_1$ on the $^3B_1$ spectrum can be understood.

The curves shown in Figure 2 depict the EOM-CCSD energy at configurations linearly interpolated between stationary points on the molecular potential energy hypersurface. From this interpolation, approximate structures and upper bounds for the energies of the associated conical intersections (CI) or transition states (TS) are obtained and presented in the results tables and Supporting Information. Clearly, the transition state linking the $(\alpha)^3A_1$ and $(\beta)^3A_1$ structures requires very little activation energy to be reached from $(\beta)^3A_1$; indeed, no transition state is predicted at all by CIS calculations from which the analogous curve is qualitatively similar in shape but is monotonic decreasing in this region. The conical intersection (C_{2v} symmetry) and transition state (C_s symmetry) linking the two low-energy states $^3B_1$ and $(\alpha)^3A_1$ are also shown; these have reasonably high energies (above the vertical transition energies). This is indicative that, in the region near the band origins at least, these two states should not strongly perturb each other's spectrum.

6. Conclusions

On the basis of assignments from new high-temperature gas-phase spectra of the S_1 and T_1 states of pyrimidine combined with reassignments of existing spectra and extensive calculations for these and 14 other excited states, we have developed a consistent analysis of the excited-state energetics and vibronic coupling of pyrimidine.

A reassignment of the triplet manifold is presented on the basis of vertical excitation energies and reorganization energies evaluated using a range of the best currently available computational techniques. Using a range of techniques is essential, as is the treatment of zero-point energy effects. The computational methods have sufficient accuracy (e.g., ±0.2 eV) to permit such an assignment, but this error is still too large to permit an accurate evaluation of the vibrational frequencies of excited-state vibrational modes involved in strong vibronic coupling. However, computations do serve to indicate the qualitative features that may be expected in excited-state properties and identify when unusual behavior can be expected. A map of the lowest triplet manifold is presented that, though details such as symmetry-breaking effects and relative energies are subject to scrutiny, provides a picture of the complexity of the manifold and approximate locations and energies for transition states and conical intersections, laying the foundations for detailed studies of excited-state kinetics.

New assignments and some reassignments for several vibrational modes of the lowest singlet and triplet excited states are presented on the basis of our new spectra and computations. This has allowed details of the vibronic coupling between $^1B_1$ and the ground state, the lowest B_1 and A_2 states, and the lowest B_1 and B_2 states to be properly quantified. Knowledge of this vibronic coupling provides indirect information concerning the excited-state energy gaps, and hence we have independently verified important aspects of our reassignment of the triplet excited states.

It is well known[1,20,24] that the geometries of $^1B_1$ and $^3B_1$ are similar and possibly of C_{2v} symmetry, but only qualitative data have been available, and previously it has not been possible to demonstrate unequivocally that these states do not have double-well potential energy surfaces in antisymmetric modes that are not sufficiently deep to support zero-point vibration. By measuring and interpreting the high-temperature absorption spectra and combining the results with previous measurements, we have been able to determine the excited-state anharmonicity of many modes and hence demonstrate that the potential energy surfaces are indeed single-minimum. However, we were not able to assign unambiguously mode 4 (b_1 symmetry) for $^3B_1$, and hence we cannot confirm that this state does not undergo the out-of-plane boat distortion. Although the singlet and triplet manifolds are in general similar, implying that the vibronic coupling to $^3B_1$ and $^1B_1$ should be similar, the B_1-to-A_1 energy gaps are much lower in the triplet manifold, and hence vibronic coupling through the active coupling vibration, mode 4, could be very different. Further experimental work to identify mode 4 unambiguously is required, as plausible scenarios based on the current work lead to conflicting conclusions concerning the existence of the boat distortion in $^3B_1$.

The conclusion that the potential energy surfaces of $^1B_1$ and $^3B_1$ do not have a double-minimum structure in the in-plane distortion mode 6b is significant in that this shows that the (π^*, n) excitation is delocalized over *both* nitrogen atoms. It is usually believed that, for diazines in solution [52] (and, incorrectly,[50] also in the gas phase for pyrazine[51]), the excitation localizes onto one nitrogen atom. Hydrogen bonding increases the tendency

for the excitation to localize. This significantly strengthens the hydrogen bond,[53,54] and a thorough knowledge of the vibronic coupling of the parent molecule is required before the properties of excited-state hydrogen bonding can be considered.

Our calculations also reveal that the lowest $^3A_1$ (π^*, π) state has a double-well structure in the totally symmetric vibration 8a. Each well corresponds to a single-determinant excitation, indicating that the pseudoparity selection rule,[47] which describes the (π^*, π) spectroscopy of alternate polyenes, does not apply. An analogous result has also been found for pyridine.[3]

Acknowledgment. P.W. gratefully acknowledges the receipt of an Internal Research Grant from the University of Western Sydney, Hawkesbury, and J.R.R. and Z.-L.C. gratefully acknowledge support from the Australian Research Council. We thank Dr. Ajith Perera from the University of Florida, Gainesville, for performing the EOM-CCSD(T) calculations.

Supporting Information Available: Details of the active spaces used in the CASSCF and CASPT2 calculations. EOM-CCSD, CCSD, TD-B3LYP, B3LYP, CASSCF, CASPT2, and CIS calculated properties of the ground state and the lowest eight excited singlet and eight triplet states of pyrimidine. Zero-point energy (ZPE) corrections. Revised harmonic and (diagonal) anharmonically corrected vibrational frequencies, zero-point energies, and estimated asymmetric contributions to the reorganization energy. Observed and simulated spectra. Franck−Condon factors for the $6a_0^1$ and $6b_0^2$ modes. This material is available free of charge via the Internet at http://pubs.acs.org.

References and Notes

(1) Innes, K. K.; Ross, I. G.; Moomaw, W. R. *J. Mol. Spectrosc.* **1988**, *132*, 492.
(2) Chachisvilis, M.; Zewail, A. H. *J. Phys. Chem. A* **1999**, *103*, 7408.
(3) Cai, Z.-L.; Reimers, J. R. *J. Phys. Chem. A* **2000**, *104*, 8389.
(4) Wormell, P.; Gready, J. E. *Chem. Phys.* **1994**, *179*, 55.
(5) Muiño, P. L.; Callis, P. R. *J. Chem. Phys.* **1994**, *100*, 4093.
(6) Buma, W. J.; Donckers, M. C. J. M.; Groenen, E. J. J. *J. Am. Chem. Soc.* **1992**, *114*, 9544.
(7) Malmqvist, P.-A.; Roos, B. O.; Fülscher, M. P.; Rendell, A. P. *Chem. Phys.* **1992**, *162*, 359.
(8) Fülscher, M. P.; Andersson, K.; Roos, B. O. *J. Phys. Chem.* **1992**, *96*, 9204.
(9) Bauernschmitt, R.; Ahlrichs, R. *Chem. Phys. Lett.* **1996**, *256*, 454.
(10) Del Bene, J. E.; Watts, J. D.; Bartlett, R. J. *J. Chem. Phys.* **1997**, *106*, 6051.
(11) Nooijen, M. *Spectrochim. Acta, Part A* **1999**, *55*, 539.
(12) Tozer, D. J.; Amos, R. D.; Handy, N. C.; Roos, B. O.; Serrano-Andrés, L. *Mol. Phys.* **1999**, *97*, 859.
(13) Fischer, G.; Wormell, P. *Chem. Phys.* **2000**, *257*, 1.
(14) Fischer, G. *Can. J. Chem.* **1993**, *71*, 1537.
(15) Weber, P.; Reimers, J. R. *J. Phys. Chem. A* **1999**, *103*, 9821.
(16) Weber, P.; Reimers, J. R. *J. Phys. Chem. A* **1999**, *103*, 9830.
(17) Palmer, M. H.; Walker, I. C.; Guest, M. F.; Hopkirk, A. *Chem. Phys.* **1990**, *147*, 19.
(18) Knight, A. E. W.; Lawburgh, C. M.; Parmenter, C. S. *J. Chem. Phys.* **1975**, *63*, 4336.
(19) Lord, R. C.; Marston, A. L.; Miller, F. A. *Spectrochim. Acta* **1957**, *9*, 113.
(20) Hochstrasser, R. M.; Marzzacco, C. J. *J. Mol. Spectrosc.* **1972**, *42*, 75.
(21) Nonhof, C. J.; van der Waals, J. H. *Chem. Phys. Lett.* **1982**, *92*, 581.
(22) Takemura, T.; Uchida, K.; Fujita, M.; Shindo, Y.; Suzuki, N.; Baba, H. *Chem. Phys. Lett. 73*, 12.
(23) Fujita, M.; Ohta, N.; Takemura, T.; Baba, H. *Bull. Chem. Soc. Jpn.* **1988**, *61*, 1787.
(24) Ottinger, C.; Vilesov, A. F.; Winkler, T. *Chem. Phys. Lett.* **1993**, *208*, 299.
(25) Bent, D. V.; Hayon, E.; Moorthy, P. *J. Am. Chem. Soc.* **1975**, *97*, 5065.
(26) Walker, I. C.; Palmer, M. H. *Chem. Phys.* **1991**, *153*, 169.
(27) Palmer, M. H.; Walker, I. C. *Chem. Phys.* **1991**, *157*, 187.
(28) Walker, I. C.; Palmer, M. H.; Ballard, C. C. *Chem. Phys.* **1972**, *167*, 61.
(29) Palmer, M. H.; Walker, I. C.; Guest, M. F.; Siggel, M. R. F. *Chem. Phys.* **1995**, *201*, 381.
(30) Innes, K. K.; McSwiney, H. D., Jr.; Simmons, J. D.; Tilford, S. G. *J. Mol. Spectrosc.* **1969**, *31*, 76.
(31) O'Brien, J. J.; Fischer, G.; Selinger, B. K. *Chem. Phys.* **1987**, *117*, 275.
(32) Pongor, G.; Fogarasi, G.; Magdó, I.; Boggs, J. E.; Keresztury, G.; Ignatyev, I. *Spectrochim. Acta, Part A* **1992**, *48*, 111.
(33) Ellis, R. L.; Kuehnlenz, G.; Jaffé, H. H. *Theor. Chim. Acta* **1972**, *26*, 131.
(34) Hegarty, D.; Robb, M. A. *Mol. Phys.* **1979**, *38*, 1795.
(35) Dunning, T. H., Jr. *J. Chem. Phys.* **1989**, *90*, 1007.
(36) Purvis, G. D., III.; Bartlett, R. J. *J. Chem. Phys.* **1982**, *76*, 1910.
(37) Stanton, J. F.; Gauss, J.; Watts, J. D.; Nooijen, M.; Oliphant, N.; Perera, S. A.; Szalay, P. G.; Lauderdale, W. J.; Gwaltney, S. R.; Beck, S.; Balková, A.; Bernholdt, D. E.; Baeck, K. K.; Rozyczko, P.; Sekino, H.; Hober, C.; Bartlett, R. J. *ACES-II*
(38) Stanton, J. F.; Bartlett, R. J. *J. Chem. Phys.* **1993**, *98*, 7029.
(39) Helgaker, T.; Jensen, H. J. A.; Joergensen, P.; Olsen, J.; Ruud, K.; Aagren, H.; Andersen, T.; Bak, K. L.; Bakken, V.; Christiansen, O.; Dahle, P.; Dalskov, E. K.; Enevoldsen, T.; Fernandez, B.; Heiberg, H.; Hettema, H.; Jonsson, D.; Kirpekar, S.; Kobayashi, R.; Koch, H.; Mikkelsen, K. V.; Norman, P.; Packer, M. J.; Saue, T.; Taylor, P. R.; Vahtras, O. *Dalton*
(40) Andersson, K.; Malmqvist, P.-Å.; Roos, B. O. *J. Chem. Phys.* **1992**, *96*, 1218.
(41) Andersson, K.; Blomberg, M. R. A.; Fülscher, M. P.; Karlström, G.; Lindh, R.; Malmqvist, P.-Å.; Neogrády, P.; Olsen, J.; Roos, B. O.; Sadlej, A. J.; Seijo, L.; Serrano-Andrés, L.; Siegbahn, P. E. M.; Widmark, P. O. *MOLCAS*, 1997.
(42) Becke, A. D. *J. Chem. Phys.* **1993**, *98*, 5648.
(43) Frisch, M. J.; Trucks, G. W.; Schlegel, H. B.; Scuseria, G. E.; Robb, M. A.; Cheeseman, J. R.; Zakrzewski, V. G.; Montgomery, J. A., Jr.; Stratmann, R. E.; Burant, J. C.; Dapprich, S.; Millam, J. M.; Daniels, A. D.; Kudin, K. N.; Strain, M. C.; Farkas, O.; Tomasi, J.; Barone, V.; Cossi, M.; Cammi, R.; Mennucci, B.; Pomelli, C.; Adamo, C.; Clifford, S.; Ochterski, J.; Petersson, G. A.; Ayala, P. Y.; Cui, Q.; Morokuma, K.; Malick, D. K.; Rabuck, A. D.; Raghavachari, K.; Foresman, J. B.; Cioslowski, J.; Ortiz, J. V.; Stefanov, B. B.; Liu, G.; Liashenko, A.; Piskorz, P.; Komaromi, I.; Gomperts, R.; Martin, R. L.; Fox, D. J.; Keith, T.; Al-Laham, M. A.; Peng, C. Y.; Nanayakkara, A.; Gonzalez, C.; Challacombe, M.; Gill, P. M. W.; Johnson, B. G.; Chen, W.; Wong, M. W.; Andres, J. L.; Head-Gordon, M.; Replogle, E. S.; Pople, J. A. *Gaussian 98*; Gaussian, Inc.: Pittsburgh, PA, 1998.
(44) Ahlrichs, R.; Bär, M.; Baron, H. P.; Bauernschmitt, R.; Böcker, S.; Ehrig, M.; Eichkorn, K.; Elliot, S.; Haase, F.; Häser, M.; Horn, H.; Huber, C.; Huniar, U.; Kattannek, M.; Kölmel, C.; Kollwitz, M.; Ochsenfeld, C.; Öhm, H.; Schäfer, A.; Schneider, U.; Treutler, O.; von Arnim, M.; Weigend, F.; Weis, P.; Weiss, H. *TURBOMOLE-4.0*; Quantum Turbomole Chemistry Group, University of Karlsruhe: Karlsruhe, Germany, 1997.
(45) Foresman, J. B.; Head-Gordon, M.; Pople, J. A.; Frisch, M. J. *J. Phys. Chem.* **1992**, *96*, 135.
(46) Reimers, J. R. *J. Chem. Phys.* **2001**, *115*, 9103.
(47) Coulson, C. A.; Richardson, G. S. *Philos. Soc.* **1940**, *36*, 193.
(48) Bolovinos, A.; Tsekeris, P.; Philis, J.; Phantos, E.; Andritsopoulos, G. *J. Mol. Spectrosc.* **1984**, *103*, 240.
(49) Donckers, M. C. J. M.; Gorcester, J.; Groenen, E. J. J.; Schmidt, J. *J. Chem. Phys.* **1992**, *97*, 99.
(50) Zeng, J.; Woywod, C.; Hush, N. S.; Reimers, J. R. *J. Am. Chem. Soc.* **1995**, *117*, 8618.
(51) Kleier, D. A.; Martin, R. L.; Wadt, W. R.; Moomaw, W. R. *J. Am. Chem. Soc.* **1982**, *104*, 60.
(52) Baba, H.; Goodman, L.; Valenti, P. C. *J. Am. Chem. Soc.* **1966**, *88*, 5410.
(53) Zeng, J.; Hush, N. S.; Reimers, J. R. *J. Chem. Phys.* **1993**, *99*, 1495.
(54) Zeng, J.; Hush, N. S.; Reimers, J. R. *J. Chem. Phys.* **1993**, *99*, 1508.
(55) Cradock, S.; Liescheski, P. B.; Rankin, D. W. H.; Robertson, H. E. *J. Am. Chem. Soc.* **1988**, *110*, 2758.
(56) Sadlej, A. J. *Collec. Czech. Chem. Commun.* **1988**, *53*, 1995.
(57) Haettig, C.; Christiansen, O.; Coriani, S.; Jogensen, P. *J. Chem. Phys.* **1998**, *109*, 9237.
(58) Callis, P. R.; Scott, T. W.; Albrecht, A. C. *J. Chem. Phys.* **1981**, *75*, 5640.
(59) Martin, J. M. L.; Alsenoy, C. V. *J. Phys. Chem.* **1996**, *100*, 6973.
(60) Scott, A. P.; Radom, L. *J. Phys. Chem.* **1996**, *100*, 16502.
(61) Sugahara, Y.; Mikami, N.; Ito, M. *J. Phys. Chem.* **1986**, *90*, 5619.